# P2.9 TOTAL LIGHTNING CHARACTERISTICS AND INFERRED CHARGE STRUCTURE OF ORDINARY CONVECTION

Shane M Motley[1], Lawrence D Carey[1*], and Martin J. Murphy[2]

[1]Texas A&M University, College Station, Texas

[2]Vaisala Corporation, Tucson, Arizona

## 1. INTRODUCTION

With the advent of continuously operational three-dimensional (3-D) lightning mapping systems, complete observations of a thunderstorm's lightning development are now routinely available. Recent studies examining correlations between three dimensional (3-D) lightning flash characteristics and convective intensity (e.g., magnitude of updraft) and state (e.g., early, mature and dissipating phases) have shown promising results; however, emphasis has focused primarily on complex modes of convection (e.g., supercells and squall lines), often with only a limited portion of the cell's lifetime examined (e.g., Ray et al. 1987; Coleman et al. 2003; Lang et al. 2004a,b; Carey et al. 2005; Wiens et al. 2005; Steiger et al. 2005). Although it is the most ubiquitous and fundamental cell type, ordinary, single-cell convection has received relatively little recent attention in the lightning community. Placing emphasis on ordinary convection allows for a more direct approach to the complex evolution of the microphysical and kinematic processes involved in the electrical development of thunderstorms.

Devising methods to associate the evolution of lightning and inferred charge structure to convective intensity and state requires an accurate and detailed depiction of 3-D total lightning data. Utilizing instruments that locate lightning radiation at VHF frequencies (very high frequency) enables the in-cloud parts of both intracloud (IC) and cloud to ground (CG) flashes to be studied. In addition, inferences on storm charge structure are possible with the use of VHF source densities (Mazur et al. 1997; Rison et al. 1999; Thomas et al. 2001) because the negative end of a bidirectional leader produces large amounts of VHF radiation (Shao and Krehbiel, 1996). Therefore, regions of high VHF source densities suggest areas of positive charge regions.

Past studies suggest that the gross charge structure of a thunderstorm resembles a dipole or tripole structure of charge with the main negative charge region located around the -10ºC to -20ºC isotherm (e.g., Williams 1989; MacGorman and Rust 1998). However, it is understood that more complex vertical charge structures can exist within convection, with up to 4 or 5 layers of charge (Stolzenburg et al. 1998). These additional charge structures are likely due to screening layers that develop as a result of discontinuities in conductivity at the boundary of clouds (MacGorman and Rust 1998). Typically, the layers of charge associated with screening layers are very thin and, unlike main charge regions, the locations of screening layers are difficult to asses with VHF lightning observations. Therefore, our emphasis will focus on the development of the gross charge structure of the conventional tripole model.

Mounting evidence suggests that the origin of the main negative charge region is the ice-ice collisional (or non-inductive) charging mechanism (e.g., Takahashi 1978). Rebounding collisions between graupel and ice crystals in the presence of supercooled water result in the particle scale separation of charge with negative (positive) charge on the graupel (ice crystal). Differential sedimentation and an increasing updraft speed with height result in the storm scale separation of charge and the classical thunderstorm dipole of positive over negative charge.

Most intracloud (IC) lightning flashes originate between the main negative and the upper positive charge regions (Shao and Krehbiel 1996). Several studies have documented this prevalence of IC lightning over CG lightning in the early stages of convective development. Williams et al. (1989) suggests this relationship is due to the accumulation of graupel particles in the center of the dipole region in the developing and mature stages of thunderstorms and the subsequent descent of ice particles below the height of the negative charge region as downdrafts begin to dominate. This subsequent decent of ice particles is attributed to the development of a lower positive charge region via the non-inductive and/or inductive (MacGorman and Rust 1998) charging mechanisms. Past research suggests that the lower positive charge region provides the bias necessary for the onset of negative polarity CG flashes (e.g., Williams 1989). Supporting the Williams et al. (1989) results, Carey and Rutledge (1996) found a strong correlation between polarimetric radar inferred graupel volume and the IC flash rate. This study also found relations between the polarity of the electrical field and the amount and vertical location of ice within the storm. These ideas suggest that correlations may exist between the state of a thunderstorm (e.g. intensifying, weakening) and total lightning data. Examination of a statistically significant quantity of air mass thunderstorms allows further exploration of the conventional model for the development of gross charge layers and lightning development. In addition it is possible to examine whether significant correlations exist between lightning

* *Corresponding author address*: Dr. Larry Carey, Dept. Atmospheric Sciences, Texas A&M University, College Station, Texas 77843-3150; larry_carey@tamu.edu

flash characteristics and radar inferred convective intensity and state.

Hypothesizing significant correlations between total flash characteristics and convective cell structure, intensity and state, we examined time-height cross-sections of mean radar reflectivity, flash origin heights, and VHF source density during the entire lifecycle of each convective cell. Total and CG lightning flash rate were also plotted in conjunction with the flash origin information in effort to gain further insight on the evolution of total lightning.

## 2. DATA AND METHODOLOGY

We employed KFWS level-II WSR-88D archive data from the National Climatic Data Center (NCDC); CG flash location, time and polarity from the National Lightning Detection Network (NLDN: owned and operated by Vaisala); and the time and three-dimensional location of VHF radiation sources associated with total lightning as measured by Vaisala's Dallas-Fort Worth Lightning Detection and Ranging (LDAR-II) network for several ordinary convective cells that occurred from May of 2001 to August of 2005. The data from both the NLDN and LDAR-II combine to form a complete dataset of total lightning data. The two-dimensional NLDN data provide the latitude-longitude location and time, polarity, and stroke multiplicity of cloud-to-ground flashes. These data were obtained from Vaisala, Inc., Tucson, AZ, which has established a network consisting of 106 sensors across the U.S. (Orville and Huffines 1999). The median accuracy of ground flash locations is approximately 500 m and the expected flash detection efficiency is > 85-90%, for events with peak currents above 5kA (Cummins et al. 1998). For our analysis, the NLDN data were post-processed such that individually recorded strokes were grouped into flashes. In addition, we removed positive flashes characterized by peak currents less than 10kA since these flashes are likely associated with misidentified IC lightning (Cummins et al. 1998; Wacker and Orville 1999a,b).

The VHF radiation produced by both IC flashes and the IC component of CG flashes is monitored by the LDAR-II network. This network is comprised of 7 VHF sensors with 20-30 km baselines centered on the Dallas-Fort Worth International Airport (e.g., Carey et al. 2005). This system monitors VHF sources which are produced during the breakdown process, marking the initiation of bipolar streamers (McGorman and Rust 1998). According to Loeb (1966), when the streamer amasses enough electrons, it becomes self-propagating with both positive and negative streamers occurring simultaneously and initiating in regions where the electric field is the highest (Coleman et al. 2003). The LDAR-II can readily detect the negative end of the leader due to the large amounts of VHF radiation produced during its development (Shao and Krehbiel 1996). Continuously propagating positive leaders, on the other hand, do not emit much VHF radiation and are often missed by the LDAR system (Proctor et al. 1988). Positive and negative ends of the discharge tend to propagate through regions of extrema in the electric potential profile that approximately correspond to regions of concentrated charge of the opposite polarity (Shao and Krehbiel 1996; Coleman et al. 2003). Therefore, given that the negative polarity breakdown, which the LDAR can easily detect, typically occurs in positive charge regions, the LDAR network becomes a useful tool for inferring gross charge structure within thunderstorms.

Detecting VHF radiation sources through time of arrival systems like the LDAR-II network still comes with its limitations. These limitations must be taken into consideration before more subtle inferences of charge structure can be made. One of the most important limitations to consider is the relative detection efficiency of VHF sources. The LDAR-II network can accurately map out flashes in 3-D within approximately 100 km of the center of the network, where the expected flash detection efficiency is greater than 90% (Carey et al. 2005). Another relevant measure of performance is the source detection efficiency which was estimated to be approximately 4% of its maximum value at 100 km (Carey et al. 2005). Therefore, convective cells that did not remain within 100 km from the center of the LDAR-II network throughout their lifetime were not included in this study. This limitation in the LDAR-II network was taken into careful consideration when making inferences of charge structure and total flash characteristics. Another limitation of the LDAR-II comes from the fact that the network is not particularly good at mapping radiation sources associated with stepped and dart leaders propagating toward the ground (Mazur et al. 1997). In addition, while the breakdown and ionization processes emit strongly in VHF, CG return strokes, which occur in previously ionized channels, emit in the Low Frequency (LF) to Very Low Frequency (VLF) range. Thus, time of arrival systems like the LDAR-II are primarily limited to registering the VHF radiation associated with the IC component of total lightning.

Grouping VHF source data into individual flashes was accomplished with the use of a NASA based flash algorithm, which was recently translated to Interactive Data Language (IDL). This IDL program uses spatial and temporal restrictions to group the LDAR-II VHF sources into flashes. The program determines if a source was a part of a flash based on the following criteria: the maximum duration of the flash cannot exceed 3 seconds, the maximum time lag between points in a flash cannot exceed 0.5 seconds, the maximum time delay between points in a branch cannot exceed 0.03 seconds, and points must be within 5 km of each other to be considered part of the same flash.

The location, convective state (e.g. developing, mature, dissipating), kinematic and microphysical properties of each convective cell were inferred from the Dallas-Fort Worth WSR-88D (KFWS) data. Analysis of the radar data was performed using WDSS-II (Warning Decision Support System-Integrated Information) software (Hondl 2003) provided by the National Severe Storms Laboratory (NSSL). This software contains several algorithms that allow for quantitative analysis of the intensity of individual convective cells (e.g. Severe Hail Index (SHI) algorithm (Witt et al. 1998), Vertically

Integrated Liquid (VIL)). Identification and tracking of each convective cell was performed with the WDSS-II Storm Cell Identification and Tracking (SCIT) algorithm (Johnson et al. 1998). In an effort to obtain cells that were representative of air mass thunderstorms as described by Byers and Braham (1949), we employed certain criteria that were used to asses whether a cell could be a part of our sample. These criteria included:

1) DFW radar must capture the entire life span of the cell.
2) Distance from cell to center of LDAR-II network could not exceed 100 km during cell's life span.
3) Cell must remain isolated from other convective cells such that VHF sources from one cell could not enter another (tests were made for each cell in order to ensure this did not occur).
4) Cell did not undergo a merge or split during its lifetime.
5) Cell must be identified by WDSS-II algorithms for 30 minutes or greater.
6) 40 dBZ contour observed at or above -10º C level for at least one scan.
7) Cell has no appreciable tilt.

Since most convectively active days had several cells occurring at the same time, the LDAR-II data for a given day usually contained VHF source point information for a number of cells. Thus, if a cell met the required criteria it was necessary to separate the VHF sources associated with the cell of interest from the plethora of VHF sources that occurred from all cells within range of the LDAR-II network. This was performed by constructing a cylinder around each cell such that VHF sources that fell outside the bounds of the cylinder would not be associated with the cell of interest (Fig. 1a). The center and radius of each cylinder were constructed based on the ice-ice collisional (or non-inductive) charging mechanism (Takahashi, 1978). The presence of a sufficient quantity of graupel or hail, with ice crystals and supercooled water for charging, is typically associated with radar echoes approaching 30-40 dBZ between the -10º C and -20º C isotherm level (Dye et al. 1986). Previous studies have also shown that the main negative charge region typically resides around the level of the -10º C isotherm (Krehbiel 1986). Using archived Fort Worth rawinsonde data from the NCDC, the height of the -10º C isotherm was determined for each case day. WDSS-II was then used to examine the reflectivity values of each cell at the height of the -10º C isotherm. The center and radius of each cylinder were based on reflectivity values at the height of the -10º C isotherm with the center of the cylinder being placed at the maximum reflectivity value for each cell at that height. The radius of each cylinder extended out to the furthest 20 dBZ contour from the cell's center in effort to capture the most electrically active portion of each cell. Fig. 1a shows one of the more difficult cases in creating the bounds of each cell due to close proximity of another developing convective cell. The bounds in this case were drawn such that the locations of the flash origins, which typically reside in close proximity to the main negative charge region (Proctor 1991) for the cell of interest were separated by a considerable distance (in this case ~8km) from other cells. Latitude and longitude information for the center of each cylinder was recorded using output from WDSS-II. This information was then combined with the flash output from the NASA flash algorithm such that only those flashes that had origins within the bounds of the cell were associated with the cell. Comparisons could then be made between radar reflectivity values and total lightning data (i.e. LDAR-II source points and CG data) by converting radar data from a polar to a Cartesian grid space using REORDER software (Oye and Case 1995) and overlaying both data sets. Horizontal and vertical grid spacing for the reflectivity data were typically set at 2.0 km and 1.0 km, respectively. The relatively large grid spacing was necessitated by the routine use of the Volume Coverage Pattern-21 (VCP-21) by the KFWS WSR-88D. VCP-21, or precipitation mode, was the most common scanning strategy used, which ultimately resulted in a few data gaps in the vertical reflectivity data. Despite these occasional gaps in the radar data, the smoothing creates a general idea of the vertical distribution of reflectivity values such that the two datasets (total lightning activity and radar reflectivity) can be overlaid.

Several IDL programs were employed to compare various radar parameters against the cell total and vertical profile of flash density, flash origin density, and flash source density for several air mass thunderstorm cases. All data sets were placed on the same temporal scale such that accurate comparisons between data sets could be made. VHF source densities were normalized over a 5 minute period while CG and IC flash rates were smoothed using a 5-minute running average. The VHF source density was gridded at 1 km resolution in the vertical for time-height cross-sections. The flash algorithm was used to obtain the exact time and height of each flash origin, which was then overlaid on the radar reflectivity and VHF source density plots.

## 3. RESULTS

Two individual case studies are presented here. The first cell of interest, hereafter referred to as "cell 1," occurred on 5 August 2005, and the second cell of interest, hereafter referred to as "cell 2," occurred on 27 June 2001. Cell 1 was located 57 kilometers to the north-north east of the center of the LDAR network, with the first radar reflectivity returns occurring at 1745 UTC. The vertical structure of cell 1 at peak intensity is shown in Fig. 1b. Cell 2 was located 68 kilometers to the northeast of the LDAR center, with first radar reflectivity returns occurring at 1422 UTC. The vertical structure of cell 2 during the mature phase was shown earlier in Fig. 1a.

### *a. CELL 1*

Upper air data for 5 August 2005 were obtained from the 12 UTC Dallas-Fort Worth (FWD) rawindsonde. Conditions on this day were marginally favorable for the

development of air mass thunderstorms with 327 J $kg^{-1}$ of Convective Available Potential Energy (CAPE), and a weakly sheared vertical wind profile. The height of the -10º C and -20º C isotherms were 6.0 km and 7.7 km above ground level, respectively.

As shown in Fig. 2a, the first VHF sources that were observed by the LDAR-II occurred approximately 22 minutes after the first radar echoes associated with the storm appeared (initiation; t = 0). This time coincided with radar reflectivity inferred rapid intensification, which occurred 24 minutes (t = 24 minutes) after initiation and was marked by the 30 dBZ core rising well above the -10º C isotherm (Fig. 2a). Several other radar parameters suggest a rapid intensification occurred around this time with VIL increasing from 5 to 13 kg $m^{-2}$, and a severe hail index (SHI) of 3 J $m^{-1}$ $s^{-1}$ (Fig. 3a). The total flash rates at this time remained in the 1 to 2 flash per minute range and appeared to be predominately IC flashes (Fig. 2b). The one exception was a CG flash that occurred at t = 24 minutes. This flash occurred only two minutes and twenty-seven seconds after the first VHF source was registered by the LDAR-II. A noticeable increase in total flash rate occurred just after the period of rapid intensification (t = 36) with total flash rates increasing to levels as high as 10 flashes per minute (Fig 2b). A dramatic increase in the mean height of flash origins also occurred after the rapid intensification with mean heights rising from 8879 m to a mean height of 12223 m with standard deviations of 993 m and 1851 m, respectively.

Similar to the results found by Carey and Rutledge (1996), observations of the SHI values in Fig. 3a suggests this rapid increase in flash origin heights and VHF source density is due to an increase in the ice available for non-inductive charging. The increase in height of both the VHF sources and flash origin heights is most likely attributed to a rapid increase in updraft strength as inferred by the higher VIL values (Fig. 3a) and the increase in height of the 30 dBZ reflectivity contour during this time (Fig. 2a). This suggests that the increase in updraft is responsible for lofting the positive charge region to a higher elevation as found earlier by Krehbiel (1986). The bimodal distribution of VHF sources, which has been well documented in past studies (Krehbiel, 1986; Marshal and Rust, 1991; Shao and Krehbiel, 1996), was not evident until just after the intensification period. Many of the lightning flash origins closely followed the 30 dBZ contour and yet extended out to the 10 dBZ contour similar to the findings discussed by Proctor (1991).

The first sign of a low level extent of flashes occurs just after the peak convective intensity inferred from radar and marks the onset of several CG lightning flashes. As the cell starts to weaken slightly, a rapid decrease in the total flash rate occurs, while the CG flash rate increases slightly to a rate of 3 flashes per minute. A very noticeable bimodal distribution of flash origins develops with the top mode of flash origins closely following the 15 dBZ contour as the cell continues to weaken. During the dissipation phase, the total and CG lightning flash rates drop off to ≤ 1 flash per minute. Although the total flash rate and flash origin heights decrease to levels seen at the initial onset of lightning, which was a period of limited CG flash activity, many of the lightning flashes during the dissipating phase of the cell are actually CG flashes. All of these results closely follow the idea of the decent of ice particles contributing to a lower positive charge region leading to the onset of CG lightning flashes (e.g., Williams 1989; Williams et al. 1989; Carey and Rutledge 1996).

*b. CELL 2*

A minimal shear environment was again evident on the 12 UTC FWD sounding for 27 June 2001, yet substantially more instability existed as evidenced by the 1605 J $kg^{-1}$ of CAPE. The -10º C and -20º C isotherms were located at heights of 5.8 km and 7.3 km above ground level, respectively. This particular cell was located 68 kilometers northeast of the LDAR center and had a life span of approximately 85 minutes. Because of the relatively large distance of the cell from the center of the LDAR-II network, range effects, which limit the number of VHF sources observed by the LDAR-II, were taken into consideration. In addition to range effects, cell 2 was surrounded by two other cells, which required careful analysis when constructing the boundaries of the cell. Fig. 1a shows one of the more difficult times in this period when the bounds of the cell came within close proximity to a newly forming cell just to the south east of cell 2. However, the cells are well separated at and above the height of the -10º C isotherm, where most lightning production typically occurs, therefore this case passes the required criteria necessary for a valid case.

The first radar echo appeared at 1422 UTC (t = 0 minutes) with radar reflectivity data suggesting rapid intensification occurring just 10 minutes later. The 30 dBZ contour rose above the height of the -10º C isotherm at t = 6 minutes, 5 minutes prior to the first IC flash which occurred at t = 11 minutes. Contrary to the results of Williams et al. (1989), the first CG flash was observed only 2 minutes after the first IC flash was observed (t = 13 minutes), with 3 more CG flashes occurring a short time thereafter at t = 15, 17, and 18 minutes (Fig. 4a). Looking at the CG flash rate (Fig. 4b), it is interesting to note that the CG flash rates are rather high at the beginning of the cell's life span, which does not support previous studies showing a preference for a higher CG flash rate as the cell begins to weaken (e.g., Williams et al. 1989; Carey and Rutledge 1996). This difference may be partially attributed to range effects associated with the relatively large distance of the cell from the LDAR-II. The total lightning flash rate followed a more conventional pattern with a significant increase as the cell intensified. Unlike in cell 1, the mean of the flash origin heights remained around the 9.5 km level throughout much of the cell's lifespan. However, there appear to be three maxima in VHF source and flash origin density that coincide with increases in the radar inferred cell intensity (Fig. 3b). Though far less dramatic than cell 1, cell 2 still manages to show the maximum concentration of VHF source densities increase in height

during the peak intensity of the cell, subsequently descending in height as the cell weakens. Also of interest is the increase in the SHI and VIL (Fig. 3b) just prior to the peak VHF source density which occurred at t = 23 (Fig. 4a). The peak flash rate and VHF source density also seemed to lag the peak intensity by 0 to 10 minutes as inferred from VIL, SHI, and height of the 30 dBZ contour (c.f., Figs. 3b, 4a, 4b). Due to the large number of VHF sources, it is difficult to notice a bimodal distribution in the VHF source density, but careful analysis of the flash origin heights does suggest a rather prominent bimodal distribution of flash origins with one mode occurring above a height of 10 km and the other mode occurring around the 8 km level. This bimodal distribution decreases somewhat as the cell begins to approach the weakening stage with most of the flash origins closely following the 30 dBZ contour. A sudden decrease in the height of the 30 dBZ contour is noted at t = 35 minutes at which point the VHF source density and total flash rate drop significantly with flash rates dropping from 9 flashes per minute to 0.2 flashes per minute by t = 42 minutes. A slight increase in the cell's intensity occurs at t = 50 minutes (Fig 3a), which is followed by a sudden increase in total flash rate (Fig. 4b) just before the cell finally dissipates all together.

## 4. DISCUSSION AND CONCLUSIONS

Using 3-dimensional total lightning data, we have provided further evidence supporting the relationship between the convective state of thunderstorms and lightning type and location. The results from cell 1 follow results from several previous studies which show IC lightning dominating in the early stages of vertical development (Williams et al. 1989; Carey and Rutledge 1996). During the initial stages of development, the 35 dBZ contour remained well bellow the -10º C isotherm, suggesting an insufficient quantity of graupel or hail available for the non-inductive charging mechanism (Vincent and Carey, 2004). Not surprisingly, this time did not experience any lightning activity and it was not until the 35 dBZ core began to rise during the onset of rapid intensification that the first lightning flashes occurred. This result is similar to previous studies, which suggest that rapid electrical development is associated with the development of mixed-phase precipitation (i.e. graupel and ice crystals in the presence of supercooled water droplets) leading to non-inductive charging as shown by the intensification of the radar echo (e.g., Reynolds and Brook 1956; Krehbiel 1986; Williams 1989; Carey and Rutledge 1996).

For cell 1, the VHF source data suggest the main positive charge region was first approximately along the -18º C isotherm at a height of 7.6 km. As in Krehbiel (1986), this inferred charge region increased to the -30º C isotherm after the cell intensified, resulting in a significant increase in the total flash rate. This is likely due to the combined effects from the elevated dipole hypothesis (MacGorman et al. 1989) and the increased charge separation occurring in the strong updraft of the cell at this time. In addition, the SHI during this time increased to 3 J $m^{-1}$ $s^{-1}$, suggesting a sufficient amount of ice was available to induce the non-inductive charging mechanism. As the cell began to weaken, the CG flash rate increased for cell 1 associated with a descent of ice particles and the subsequent formation of a lower positive charge region as inferred by the increase in the percentage of low-level flash origins (e.g., Williams 1989; Williams et al. 1989; Carey and Rutledge 1996).

Cell 2, however, did not experience a significant change in the CG lightning flash rate but appeared rather diffuse over time. Peaks in the total flash rate, on the other hand, occurred 0 to 10 minutes after the radar inferred peaks in convective intensity for both cell 1 and cell 2. This suggests that total lightning, as opposed to CG lightning, is closely correlated to the radar inferred intensity of the cell. This has implications for operational use as real-time total lightning data could serve as an additional tool for assessing the convective intensity of thunderstorms.

Further observation of cell 2 does not suggest that the height of the main positive charge region experienced as much variability as cell 1; however, a slight increase in height was noted during the intensification period of cell 2. The lack of variability seen in cell 2 could be due to the plethora of VHF sources that occurred during the lifetime of the cell making it difficult to single out a given charge layer. However, lightning is initiated where the electric field is the strongest (MacGorman and Rust 1998) and electric fields are at a maximum between oppositely charged regions. Therefore, if we assume a thunderstorm with a tripole structure then we should expect to see a maximum in the VHF source density at a height just above the max in flash origin density. This case is seen in cell 2, which shows a max in the VHF source density located slightly above the maximum flash origin density.

Although significant trends in the VHF source density, and flash origin density are slight in cell 2, correlations between flash characteristics and radar variables are present. In the case of cell 1, however, the correlations between the flash characteristics and radar variables are quite obvious. Although the results are still preliminary, these results show that the electrical development and flash characteristics of air mass thunderstorms follow those of more complex modes of convection. However, these two particular cases were specifically chosen to show that even two cells of the most basic mode of convection can contain significant differences in their lightning characteristics. Performing more stringent guidelines on the range criteria for valid cells in our study may be necessary in order to have increased confidence in our results.

Ultimately, this research will lead to important implications for short-term operational forecasting along with an advancement of our basic understanding of cloud electrification.

## 5. REFERENCES

Byers, H. R., and R. R. Braham Jr., 1949: *The Thunderstorm.* U.S. Govt. Printing Office, 287 pp.

Carey, L. D., M. J. Murphy, T. L. McCormick, and N. W. S Demetriades, 2005: Lightning location relative to storm structure in a leading-line trailing-stratiform mesoscale convective system, J. Geophys. Res., 110, doi:10.1029/2003JD004371.

Carey, L. D. and S. A. Rutledge, 1996: A multiparameter radar case study of the microphysical and kinematic evolution of a lightning producing storm. *Metr. Atmo. Phys.,* **59**, 33-64.

Coleman, L. M., T C. Marshall, M. Stolzenburg, T. Hamilin, P.R. Krshbiel, W. Rison, and R. J. Thomas, 2003: Effects of charge and electrostatic potential of lightning propagation, J. Geophys. Res., 108(D9), 4298, doi: 10.1029/2002JD002718

Cummins, K. L., M. J. Murphy, E. A. Bardo, W. L. Hiscox, R. B. Pyle, and A. E. Pifer, 1998: A combined TOA/MDF technology upgrade of the U. S. National Lightning Detection Network. *J. Geophys. Res.*, **103,** 9035-9044.

Dye, J. E., J. J. Jones, W. P. Winn, T. A. Cerni, B. Gardiner, D. Lamb, R. L. Pitter, J. Hallett, and C. P. R. Sunders, 1986: Early electrification and precipitation development in a small, isolated Montana cumulonimbus. *J. Geophys. Res.*, **91**, 1231 – 1247.

Hondl, K. D., 2003: Capabilities and components of the Warning Decision Support System – Integrated Information (WDSS-II). Preprints, 19th *Conf. On Interactive Info. Processing Systems*, Long Beach, CA, Amer. Meteor. Soce., CD preprints.

Johnson, J. T., P.L. MacKeen, A. Witt, E. D. Mitchell, G. J. Stumpf, M. D. Eilts, and K. W. Thomas, 1998: The storm cell identification and tracking algorithm: An enhanced WSR-88D algorithm. *Wea. Forecasting,* **13,** 263-276.

Krehbiel, P. R., 1986: The electrical structure of thunderstorms, in *The Earth's Electrical Environment, Studies in Geophysics, pp*. 90-113, National, Acad. Sci. Press, Washington, D. C.

Lang, T. J., and co-authors, 2004a: The Severe Thunderstorm Electrification and Precipitation Study (STEPS). *Bull. Amer. Meteorol. Soc.*, **85**, 1107-1125.

Lang, T. J., S. A. Rutledge, K. C. Wiens, 2004b: Origins of Positive Cloud-to-Ground Lightning Flashes in the Stratiform Region of a Mesoscale Convective System. Geophysical Research Letters, 31, L10105, 10.1029/2004GL019823.

Leob, L.B., 1966: The mechanisms of stepped and dart leader in cloud-to-ground lightning strokes. *J. Geophys. Res.*, 71, 4711-4721

MacGorman, D. R., and W. D. Rust, 1998: *The Electrical Nature of Storms*, Oxford Univ. Press, New York.

MacGorman, D. R., D. W. Burgess, V. Mazur, W. D. Rust, W. L. Taylor, and B. C. Johnson, 1989: Lightning rates relative to tornadic storm evolution on 22 May 1981. *J. Atmos. Sci.,* **46,** 221-250.

Mazur, V., E. Williams, R. Boldi, L. Maier, and D.e. Proctor (1997), Initial comparison of lightning mapping with operational time of arrival and interferometric systems, *J. Geophys. Res.,* **102,** 11,071-11,085.

Orville, R. E., and G. R. Huffines, 1999: Lightning ground measurements over the contiguous United States: 1995-1997, Mon. Wea. Rev., **127**, 2693-2703.

Oye, D. and M. Case, 1995: REORDER: *A program for gridding radar data. Installation and use manual for the UNIX version*, NCAR Atmospheric Technology Division, Boulder CO, 19pp.

Proctor, D. E., 1991: Regions where lightning flashes begin. *J. Geophys. Res.*, **96**, 5099-5112.

Proctor, D. E., R. Uytenbogaardt, and B.M. Meredith, VHF pictures of lightning flashes to ground, *J. Geophys. Res.*, **93**, 12,683-12,727, 1988.

Reynolds S. E. and M. Brook, 1956: Correlation of the initial electric field and the radar echo in thunderstorms. *J. Atmos. Sci.,* 13, 376-380.

Rison, W., R. J. Thomas, P. R. Krehbiel, T. Hamlin, and J. Harlin, 1999: A GPS-based three-dimensional lightning mapping system: Initial observations in central New Mexico, *Geophys. Res. Lett,* 76, 1478 – 1489.

Shao, X. M., and P. R. Krehbiel, 1996: The spatial and temporal development of intracloud lightning, *J. Geophys., Res.,* **101,** 26,641-26,668.

Steiger, S. M., R. E. Orivlle, M. J. Murphy, and N. W. S. Demetriades, 2005: Total lightning and radar characteristics of supercells: Insights on electrification and severe weather forecasting. Amer. Meteorol. Soc., *Conference on the Meteorological Applications of Lightning Data*, Paper P1.7.

Stolzenburg, M., W. D. Rust, and T. C. Marshall, 1998: Electrical structure in thunderstorm convective regions. Part III Synthesis, *J. Geophys. Res.,* **103,** 14097-14108.

Takahashi, T., 1978: Riming electrification as a charge generation mechanism in thunderstorms. *J Atmos. Sci.*, **35**, 1536-1548.

Thomas, R. J., P. R. Krehbiel, W. Rison, T. Hamlin, J. Harlin, and D. Shown, 2001: Observations of VHF source powers radiated by lightning, Geophys. Res. Lett., 28, 143-146.

Wacker, R. S., and R. E. Orville, 1999a: Changes in measures lightning flash count and return stroke peak current after the 1994 U.S. National Lightning Detection Network Upgrade: 1. Observations, *J. Geophys. Res*., **104**, 2151-2158.

Wacker, R. S., and R. E. Orville, 1999b: Changes in measures lightning flash count and return stroke peak current after the 1994 U.S. National Lightning Detection Network Upgrade: 2. Theory, *J. Geophys. Res*., **104**, 2159-2162.

Wiens, K. C., S. A. Rutledge, and S. A. Tessendorf, 2005: The 29 June 2000 Supercell Observed During STEPS. Part II: Lightning and Charge Structure. *J. Atmos. Sci.*, **in press.**

Williams E. R., 1989: The Tripole structure of thunderstorms., *J. Geophys. Res.,* **94,** 13,151 – 13,167.

Williams E. R., M. E. Webber, R. E. Orville, 1989: The relationship between lightning type and convective state of thunderclouds., *J Geophys. Res.,* **94**, 13,213-13,220.

Witt, A., M. D. Eilts, G. J. Stumpf, J. T. Johnson, E. D. Mitchell, anb K. W. Thomas, 1998: An enhanced hail detection algorithm for the WSR-88D. *Wea. Forecasting,* **13,** 513–518.

Vincent, B. R. and L. D. Carey, 2004: Using WSR-88D reflectivity data for the prediction of cloud-to-ground lightning: A central North Carolina study., *Natl. Wea. Digst*., 35-43.

**a.**

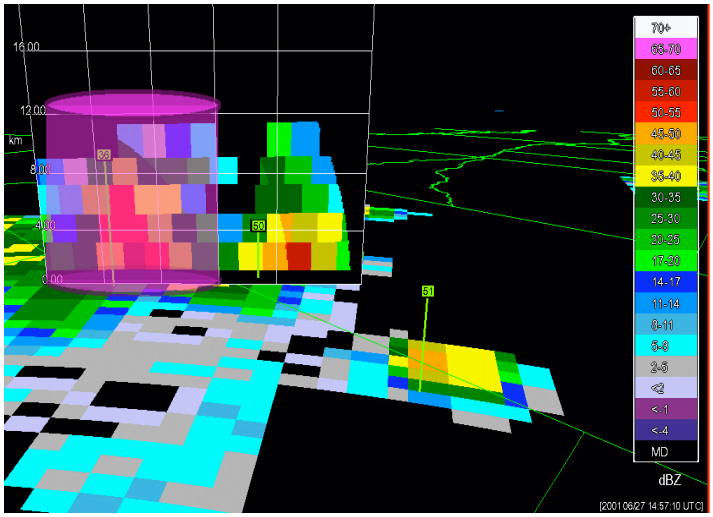


**b.**

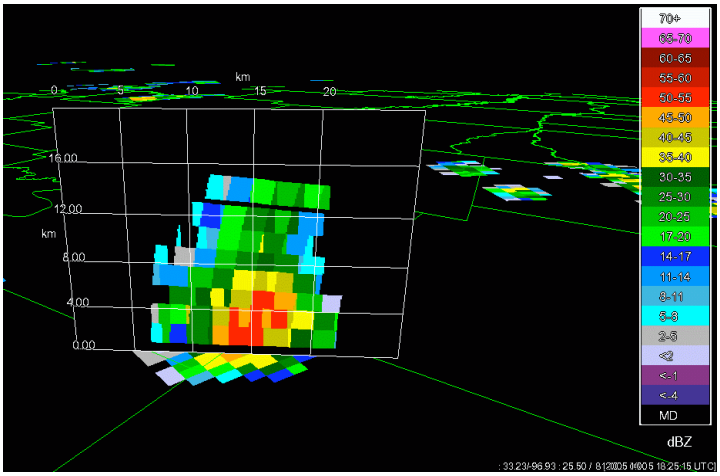


Figure 1. 3-D depiction of radar reflectivity, dBZ shown. a) Vertical cross section taken through cell 2 during peak intensity at 1457 UTC (t = 35 minutes). Shaded cylinder constructed around cell shows bounds of cell 2. Cross-section grid box spacing is 4km in the vertical plane and 5km in the horizontal plane. b) Same as (a), but for cell 1 with vertical cross section taken during peak intensity at 1825 UTC (t = 40 minutes).

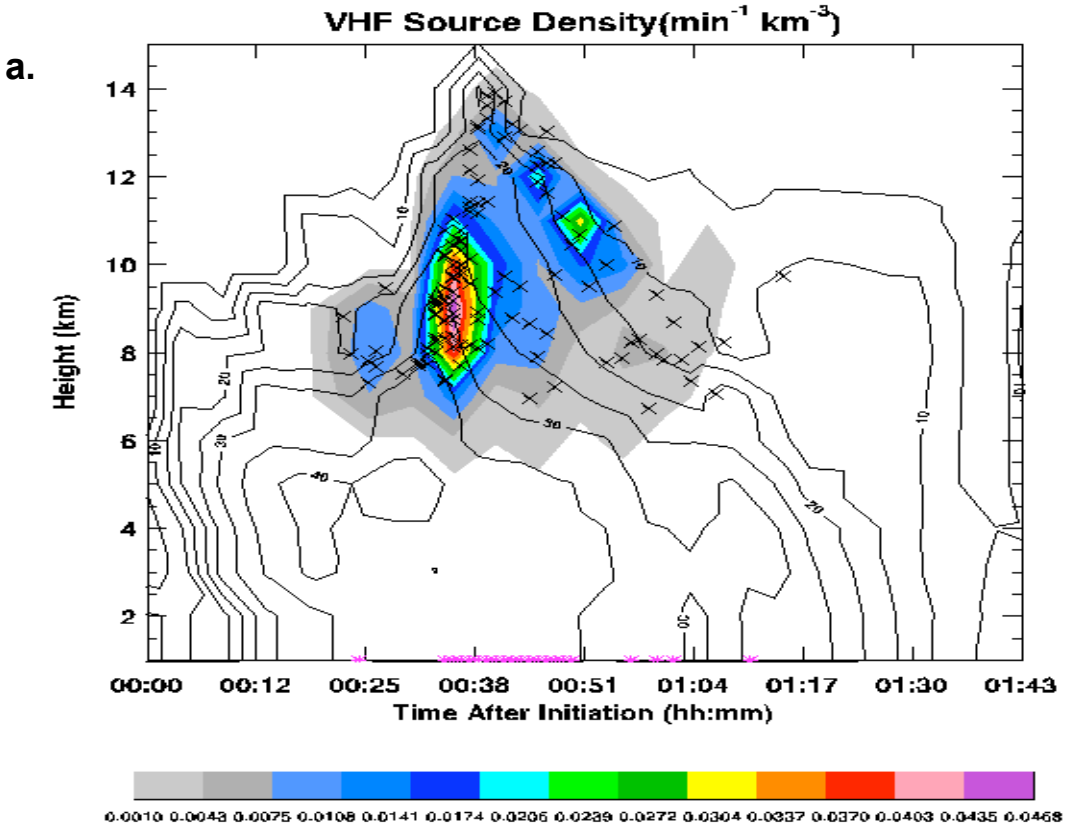


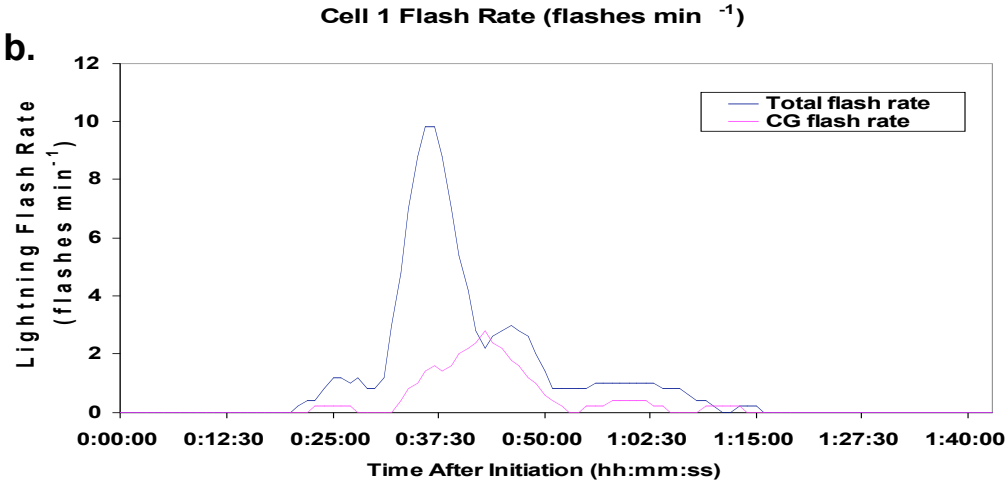


Figure 2. Radar and lightning evolution of cell 1. a) Time (after cell initiation, occurring at 1745 UTC) height (km) cross section of VHF source density (colored shading), flash origin locations (x), CG times (*), and radar reflectivity (dBZ, contoured starting at 5dBZ every 5dBZ) for cell 1. b) 5 minute running average of lightning flash rate for total lightning data (blue line) and CG flash rate (red line) of cell 1.

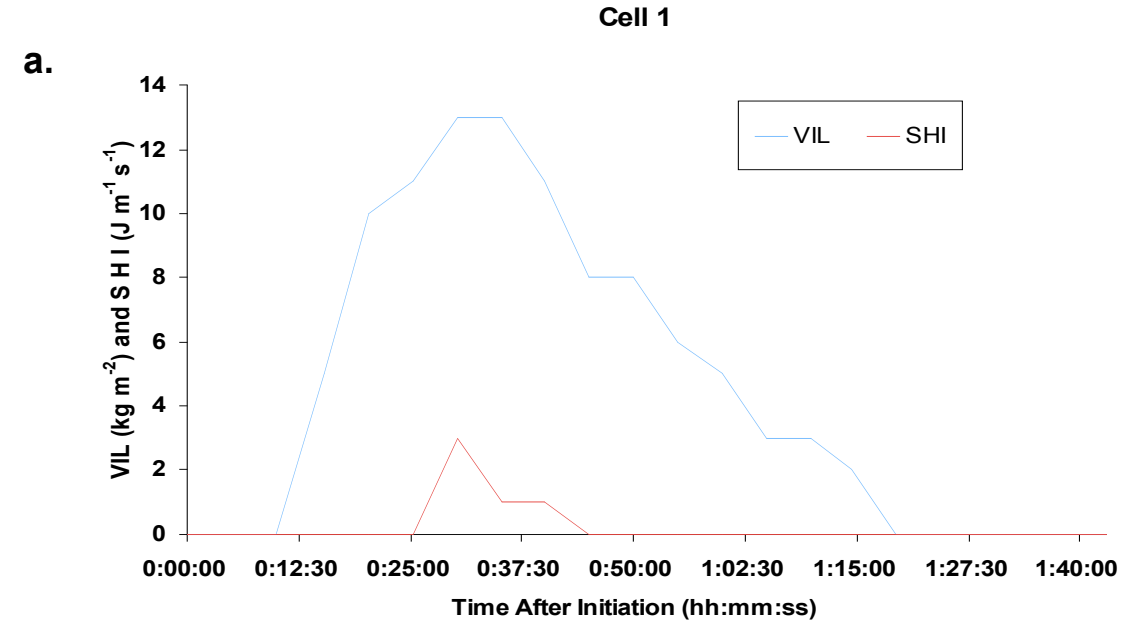


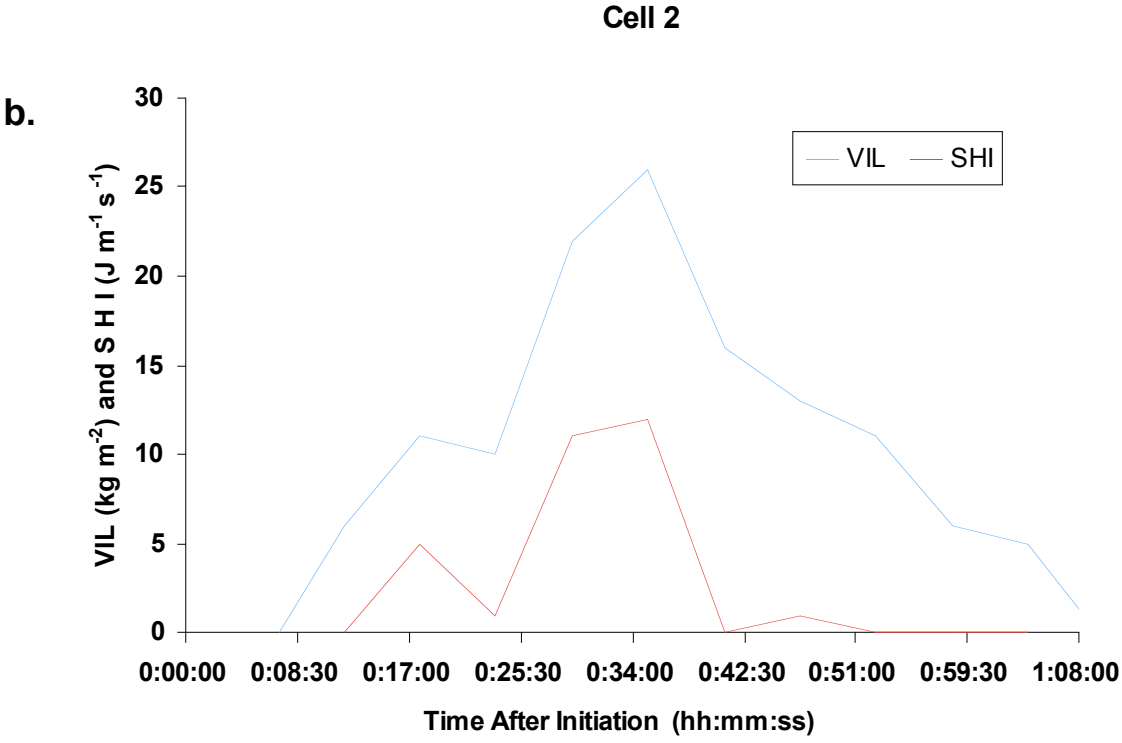


Figure 3. Temporal evolution of the radar inferred intensity parameters, Vertically Integrated Liquid (VIL, kg $m^{-2}$ ; Blue line) and Severe Hail Index (SHI, J $m^{-1}$ $s^{-1}$; Red line). a) Cell 1. b) Cell 2

a.

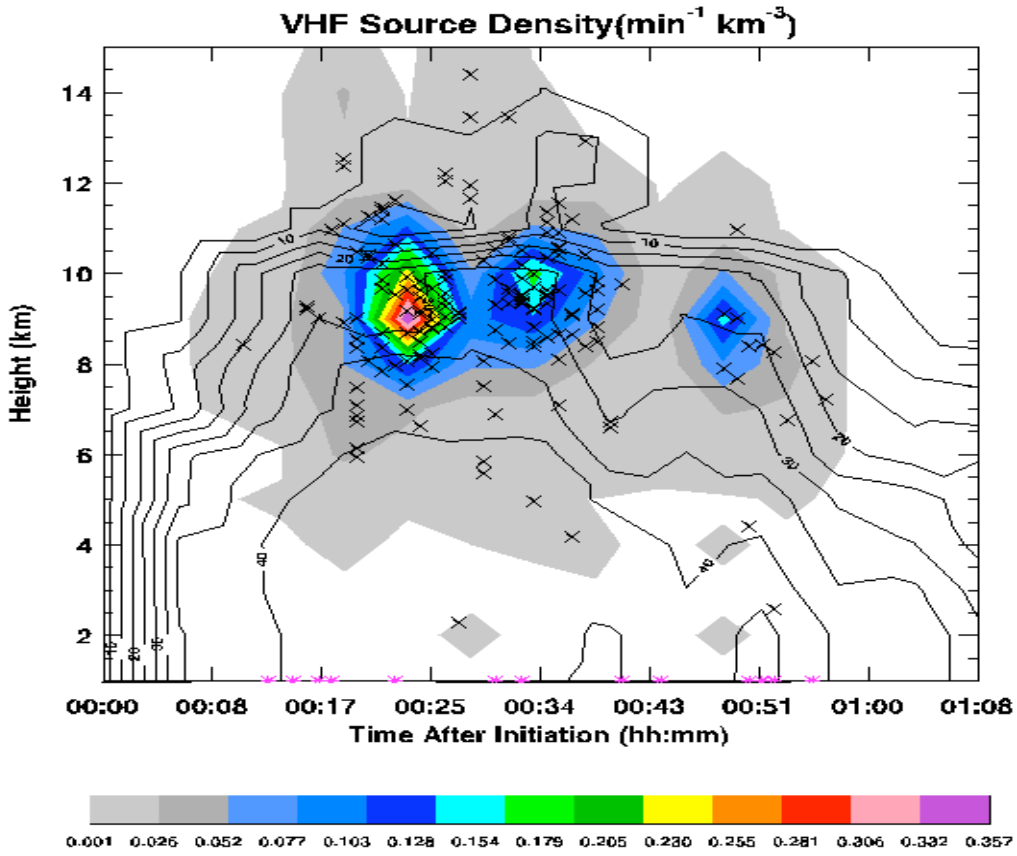


b.

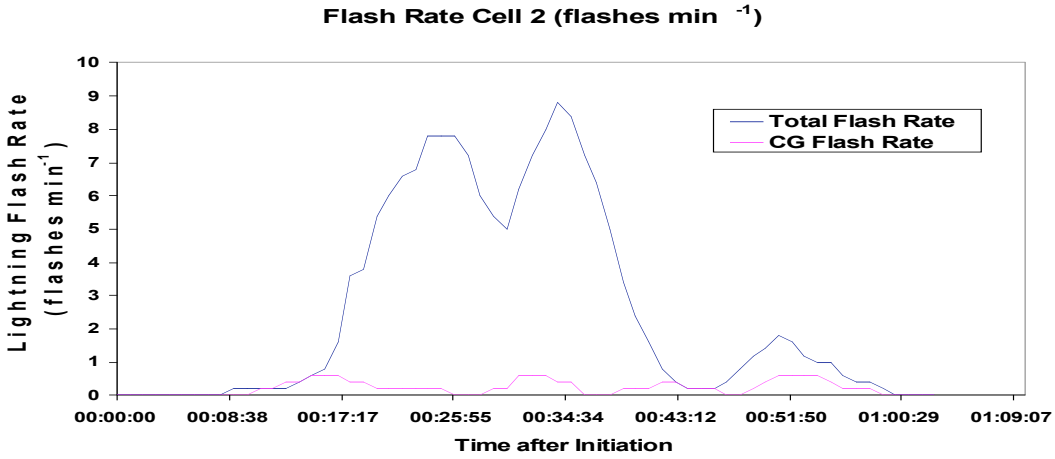


Figure 4. Radar and lightning evolution of cell 2. a) Time (after cell initiation, occurring at 1422 UTC) height (km) cross section of VHF source density (colored shading), flash origin locations (x), CG times (*), and radar reflectivity (dBZ, contoured starting at 5dBZ every 5dBZ) for cell 2. b) 5 minute running average of lightning flash rate for total lightning data (blue line) and CG flash rate (red line) of cell 2.